Available online at www.sciencedirect.com
SCIENCE DIRECT®
Journal of Sound and Vibration 276 (2004) 401–417
JOURNAL OF SOUND AND VIBRATION
www.elsevier.com/locate/jsvi

An indirect approach to investigating the dynamics of a structure containing ball bearings

P. Čermelj, M. Boltežar*

Faculty of Mechanical Engineering, University of Ljubljana, Aškerčeva 6, 1000 Ljubljana, Slovenia

Received 21 February 2003; accepted 24 July 2003

Abstract

This study introduces an integrated approach to the transmission of bearing vibrations in a generalized sense where the bearing is presented as a three-dimensional joint-model. A specially manufactured device and a corresponding analytical model are presented in order to compare experimental and numerical methods for investigating bearing transmission and bearing identification. Based on a multi-degree-of-freedom dynamic analysis, a predefined three-dimensional model of the bearing is used in a frequency domain synthesis with analytical and experimental modal analyses and FEM updating in order to obtain the system's overall dynamic properties. Such an approach separates the model of the bearing and its investigation from the remaining linear part of the whole system, which speeds up the computation and broadens the investigation's capabilities. A bearing-identification algorithm, using a perturbation approach with frequency response sensitivities and correlation analysis, is proposed, together with the required frequency response function's measurements and identification results.

1. Introduction

Over the past few decades, many approaches and results have been presented in the field of the vibration of bearings and the transmission of vibration through bearings. In this paper the discussion will be limited to deep-groove ball bearings that are part or a subsystem of a larger, more complex system. There is often a need to determine the natural frequencies and mode shapes, or even the transient responses to various inputs, of such complex systems that incorporate ball bearings. Bearings are usually used as spindle-or shaft-supporting parts that have their own dynamic properties. In order to predict a response simulation, the bearing's dynamic

*Corresponding author. Tel.: +386-1-4771-608; fax: +386-1-2518-567.
E-mail address: miha.boltezar@fs.uni-lj.si (M. Boltežar).

0022-460X/$ - see front matter
doi:10.1016/j.jsv.2003.07.039

properties are represented as a mathematical model, which should reflect the real system—the bearing—as well as possible.

Investigations of bearing dynamics and its influence on an adjoining system began many decades ago. The bearing was represented by a simple one- or two-degree-of-freedom (2-d.o.f.) model, with linear springs, and with or without damping [1,2]. Later, more refined bearing models were introduced, but the main improvement was the 5-d.o.f. bearing model from Lim and Singh [3,4]. This model assumes rigid outer and inner rings and deformable balls. Subsequent research, based on the model of Lim and Sing was still restricted to simple models, i.e., only for bearings with simple, equivalent models of adjoining systems [5–7]. A similar usage of the theoretically derived, bearing-stiffness model, in conjunction with simple models of adjoining systems, was presented by Royston and Basdogan [8] for the self-aligning, spherical ball bearing, where some of the terms from the stiffness matrix were validated experimentally. The transmission phenomena on the theoretically derived stiffness of the tapered roller bearing vibrations was studied by Bilodeau [9], whereas Rook and Singh [10] studied an integrated approach to the power flow of rolling–bearing connected structures considering bearing–adjoining-system interactions and their influence on the bearing's model definition.

Some authors investigated bearing-support models, where more detailed models were used for the adjoining systems (supports, spindles, etc.) or, alternatively, less detailed bearing models were used [11–14]. Other researchers simply studied bearing-induced vibration without transmission phenomena [15,16]. All of these analyses just mentioned were linear analyses. However, non-linear analyses investigating the bearing dynamics [17–19] are usually more complex with respect to the bearing-support model definition as well as in transmission studies.

Recent studies, in this case for studying shaft-bearing-support systems, are those with discretization principles, mainly approaches that involve distributed parameter systems [20–22], and finite-element-based analyses in conjunction with various reduction and coupling methods [12,23–25], in the numerical and experimental senses. These methods deal with m.d.o.f. systems, regardless of the type of the analytical–numerical approach used.

In this article, a m.d.o.f.-based investigation using the finite-element method, model reduction, coupling analyses, correlation, model updating, experimental work, and bearing identification is described to study the dynamic properties of a complex system involving deep-groove ball bearings. The approach proposed is an indirect one, and the bearing-model validation as well as the identification of the terms from the bearing's stiffness and damping matrices, respectively, is achieved using a special-purpose experimental device.

2. m.d.o.f. analysis and FRF coupling

2.1. Bearing model

According to the Hertzian contact theory the relation between ball displacement and the normal force for a steel-based deep-groove ball bearing can be expressed as [1,2]:

$$\delta = 4.37 \times 10^{-4} \frac{Q^{2/3}}{d^{1/3}} (\text{mm}), \tag{1}$$

when inserting the normal force, Q, in N and ball's diameter, d, in mm. Following Lim and Sing's bearing model [3], the *mean bearing displacement*, $\mathbf{q}_{bm}$, and the *mean bearing force*, $\mathbf{f}_{bm}$, are defined as (see Fig. 1):

$$\mathbf{q}_{bm} = \{\delta_{xm}, \delta_{ym}, \delta_{zm}, \beta_{xm}, \beta_{ym}\}^{\mathrm{T}}, \tag{2}$$

and

$$\mathbf{f}_{bm} = \{f_{xm}, f_{ym}, f_{zm}, m_{xm}, m_{ym}\}^{\mathrm{T}}. \tag{3}$$

δ are the displacements in m, β are the rotations in rad, f are the forces in N, and m are the moments in N m. The normal, δ_{n_j}, and radial, δ_{r_j}, displacements of the jth ball are expressed as

$$\delta_{n_j} = \delta_{zm} + r_j(\beta_{xm}\sin(\psi_j) - \beta_{ym}\cos(\psi_j)), \tag{4}$$

and

$$\delta_{r_j} = \delta_{xm}\cos(\psi_j) + \delta_{ym}\sin(\psi_j) - \gamma. \tag{5}$$

By rewriting Eq. (1) for the jth ball in the form $Q_j = K_n\delta^n$ ($n = 3/2$, δ inserted in m, and K_n in $\mathrm{N/m}^n$), where $n = \frac{3}{2}$, and defining the jth ball's displacement and contact angle α_j as (see Fig. 1):

$$\delta(\psi_j) = \begin{cases} A(\psi_j) - A_0 & \delta_j \geqslant 0, \\ 0 & \delta_j < 0, \end{cases} \quad A(\psi_j) = \sqrt{(\delta^*_{nj})^2 + (\delta^*_{rj})^2},$$
$$\delta^*_{nj} = A_0\sin\alpha_0 + \delta_{nj}, \quad \delta^*_{rj} = A_0\cos\alpha_0 + \delta_{rj}, \quad \tan\alpha_j = \delta^*_{rj}/\delta^*_{nj}, \tag{6}$$

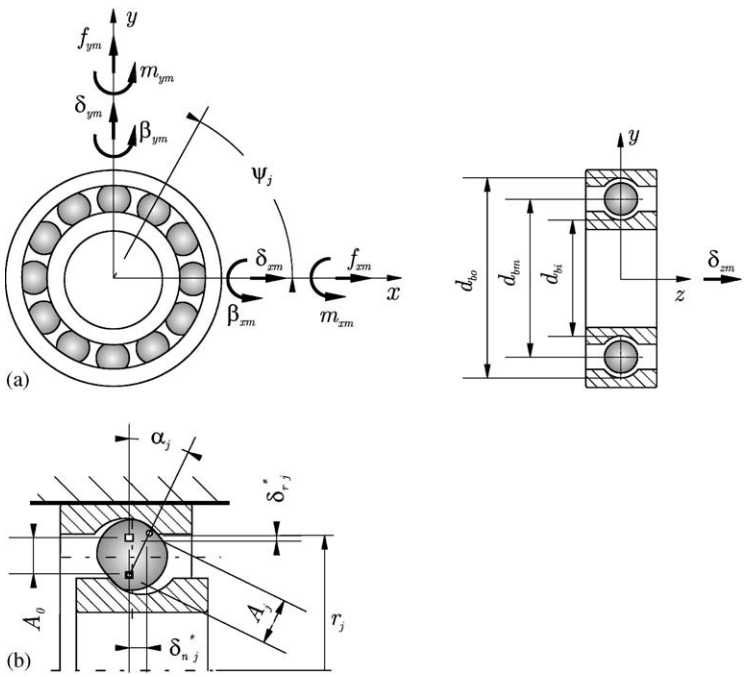

Fig. 1. Deep-groove ball bearing with dimensions and mean displacement (a); deformation of a ball under mean force (b).

the mean bearing force is obtained by summing the contributions from Z balls:

$$\mathbf{f}_{bm} = \begin{Bmatrix} \sum_{j=1}^{Z} Q_j \cos\alpha_j \cos\psi_j \\ \sum_{j=1}^{Z} Q_j \cos\alpha_j \sin\psi_j \\ \sum_{j=1}^{Z} Q_j \sin\alpha_j \\ \sum_{j=1}^{Z} r_j Q_j \sin\alpha_j \sin\psi_j \\ \sum_{j=1}^{Z} -r_j Q_j \sin\alpha_j \cos\psi_j \end{Bmatrix}. \tag{7}$$

A_0 and $A(\psi_j)$ are the unloaded and loaded distances between the inner and outer curvature centers, respectively. Finally, the 5×5 matrix of bearing stiffness is expressed as

$$\mathbf{K}_{bm} = \frac{\partial \mathbf{f}_{bm}}{\partial \mathbf{q}_{bm}} = \begin{bmatrix} k_{xx} & k_{xy} & k_{xz} & k_{x\beta_x} & k_{x\beta_y} \\ & k_{yy} & k_{yz} & k_{y\beta_x} & k_{y\beta_y} \\ & & k_{zz} & k_{z\beta_x} & k_{y\beta_y} \\ & \textit{symmetric} & & k_{\beta_x\beta_x} & k_{\beta_x\beta_y} \\ & & & & k_{\beta_y\beta_y} \end{bmatrix}. \tag{8}$$

From Eq. (8), 15 different displacement-dependent stiffness coefficients can be derived, e.g.,

$$k_{xx} = K_n \sum_{j}^{Z} \frac{(A_j - A_0)^n \cos^2\psi_j (nA_j(\delta_{rj}^*)^2/(A_j - A_0) + A_j^2 - (\delta_{rj}^*)^2)}{A_j^2}. \tag{9}$$

Usually, only the mean bearing force is known (the bearing's static pre-load), therefore, a set of 5 non-linear equations in the form

$$\mathbf{F} = \mathbf{f}_{bm_0} - \mathbf{f}_{bm}, \tag{10}$$

is used to calculate the load-dependent bearing displacement and then stiffness according to a given mean bearing force, $\mathbf{f}_{bm_0}$. Eq. (10) can be solved using the Newton–Raphson scheme. The finite-element model for $\mathbf{K}_{bm}$ is shown in Fig. 2a.

Together with the mean bearing stiffness $\mathbf{K}_{bm}$, and the force and displacement compatibility, the two-node, bearing finite-element $\mathbf{K}_{b2}$ was constructed, which also represents a

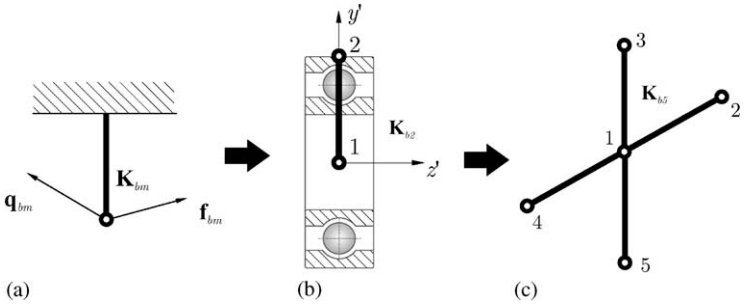

Fig. 2. Finite-element models of a bearing as $\mathbf{K}_{bm}$ (a), two-node, bearing FE (b), and five-node, bearing FE (c).

joint (Fig. 2b):

$$\mathbf{K}_{b2} = \begin{bmatrix} \mathbf{K}_{bm} & -\mathbf{K}_{bm} \\ -\mathbf{K}_{bm} & \mathbf{K}_{bm} \end{bmatrix}. \tag{11}$$

Furthermore, the two-node, bearing model was extended to a five-node, bearing model (Fig. 2c) using the sum of 4 two-node elements in a FE sense:

$$\mathbf{K}_{b5} = \sum_{j=1}^{4} \frac{1}{4} \mathbf{K}_{b2}. \tag{12}$$

A 5-d.o.f. diagonal mass matrix $\mathbf{M}_{bm}$ was constructed in an approximative way:

$$\mathbf{M}_{bm} = \begin{bmatrix} m_b/2 \begin{bmatrix} 1 & 0 & 0 \\ 0 & 1 & 0 \\ 0 & 0 & 1 \end{bmatrix} & \mathbf{0} \\ \mathbf{0} & m_b d_{bm}^2 \begin{bmatrix} 1 & 0 & 0 \\ 0 & 1 & 0 \\ 0 & 0 & 2 \end{bmatrix} \end{bmatrix}, \tag{13}$$

and extended into a 5-node FE in the same manner as the stiffness matrix. Eq. (8) will be used as an initial estimate to calculate the bearing's stiffness and the damping matrix needed in the FRF coupling analysis and in the identification algorithm as presented in subsequent sections.

2.2. Coupling of subsystems

A bearing, as a part or subsystem of a larger and more complex system, influences the overall dynamic properties of such a system, mainly because of its stiffness and damping properties. Investigating a bearing's dynamic properties directly, in the experimental sense, is a difficult job to accomplish, and the only reasonable way to investigate its influence in this case was by choosing an *indirect approach* known as the coupling approach. Coupling methods enable investigation of each subsystem to be carried out separately, numerically and/or experimentally. Although there are many coupling methods, either in the modal or the frequency domain, with each possessing some advantages and some disadvantages [26], the frequency response function (FRF) coupling methods do have some advantages, especially in cases of experimentally derived subsystem models.

For the purpose of investigating a bearing's influence using numerical and experimental indirect approaches, a 4-system model consisting of subsystems A and B, and two bearings (subsystems C and D) as shown in Fig. 3, was used. The linear subsystems A and B can be studied separately, and with an adequate level of accuracy, using the FEM or an experiment, and are therefore known; subsystems C and D (bearings) can only be investigated numerically on the basis of a predefined model. The 5-node FE bearing model from the previous section was used to be coupled (FRF coupling) with the numerically known subsystems A and B, considering rotational degrees-of-freedom at coupling interfaces.

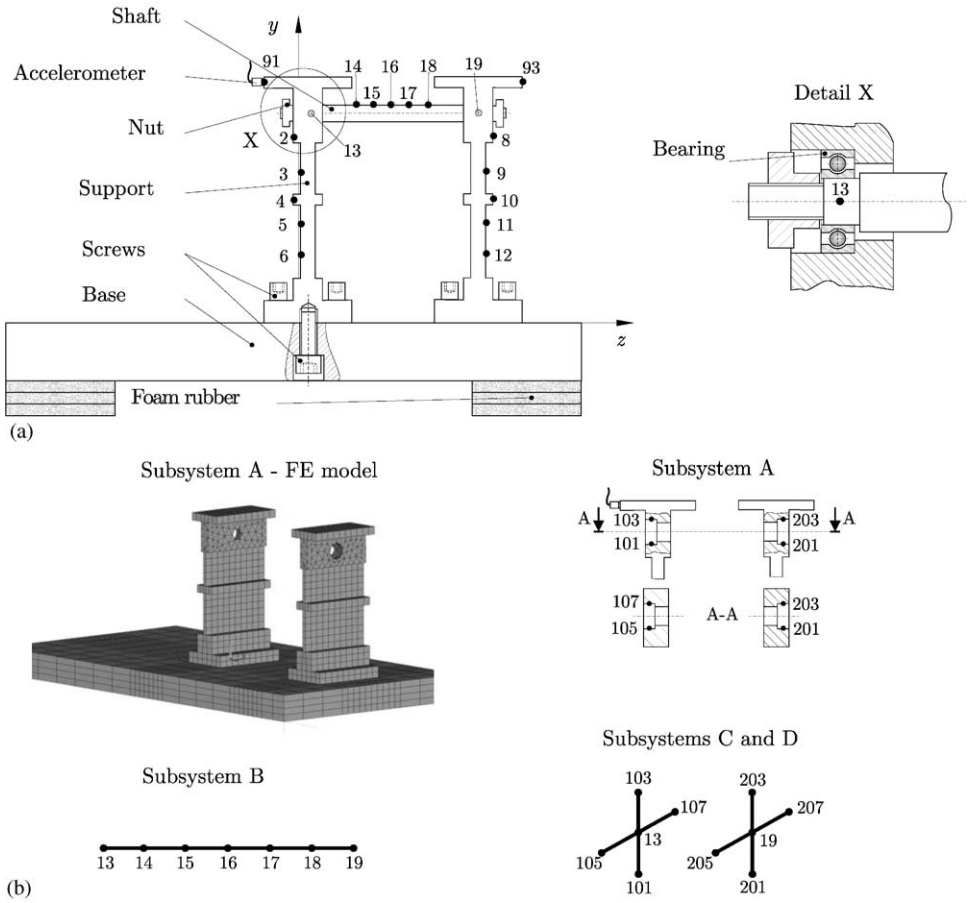

Fig. 3. Four subsystems connected (a) and connection points (nodes) along with FEM model schematics for the subsystems (b).

In general, the procedures for obtaining subsystem models depend on the coupling method used, the connection points, the d.o.f. properties, the required accuracy level, etc. To use the FRF coupling method to connect four subsystems at the connection points from Fig. 3(b) the response models of those subsystems must be provided. The response models for subsystems A and B can be derived directly from the FEM analysis. Assuming the hysteretically damped model, knowing the modal data for subsystems A and B, the modal matrices $\mathbf{\Phi}_A$, $\mathbf{\Phi}_B$, and the eigenvalue matrices $\boldsymbol{\omega}_{r_A}^2$, $\boldsymbol{\omega}_{r_B}^2$, the response model in the form of accelerance is as follows:

$$H_{jk}(\omega) = -\omega^2 \sum_{r=1}^{M} \frac{\phi_{jr}\phi_{kr}}{\omega_r^2 - \omega^2 + \mathrm{i}\eta_r\omega_r^2}. \tag{14}$$

Eq. (14) represents an approximate value for the accelerance FRF as M designates the limited number of modes used during the FRF's construction. ϕ_{rk} are the coefficients from a

mass-normalized modal matrix $\mathbf{\Phi}$ and η_r are the modal damping loss factors obtained by means of an experimental modal identification using Ewins-Gleeson's method for lightly damped systems [26] (see Table 1). The damping was identified using impact test measurements of accelerance-type FRFs on each subsystem (see Section 4.1). Alternatively, using the least-squares method, factors of the proportional Rayleigh damping, α and β, can be calculated to avoid the absence of the unmeasured η_r. A different form of the FRF model is used in such a case:

$$H_{jk}(\omega) = -\omega^2 \sum_{r=1}^{M} \frac{\phi_{jr}\phi_{kr}}{(1+\mathrm{i}\beta)\omega_r^2 - \omega^2 + \mathrm{i}\alpha}, \quad \mathbf{D} = \alpha\mathbf{M} + \beta\mathbf{K}, \tag{15}$$

with $\mathbf{D}$ as a hysteretic, proportional damping matrix.

Models for a bearing's response can, however, only be predicted when using a predefined stiffness, mass, and damping properties. Using the stiffness model from Section 2.1, the simplified mass model in the form of a diagonal matrix and a predefined proportional viscous model along with basic relations yields the bearing's response model in the form of an accelerance FRF matrix:

$$\mathbf{H}(\omega)_{b5} = -\omega^2(\mathbf{K}_{b5} + \mathrm{i}\omega\mathbf{C}_{b5} - \omega^2\mathbf{M}_{b5}), \quad \mathbf{C}_{b5} = \beta_b\mathbf{K}_{b5}. \tag{16}$$

The reason for using the basic form of FRF coupling [24,26] instead of one of the alternative forms [27] is to allow one to couple more than two systems and to derive the system's sensitivity matrix, as will be shown later (Section 3.1). Invoking the compatibility of displacements and the equilibrium of forces at the connection nodes gives us the well-known formula for the FRF of the whole, connected system $\mathbf{H}(\omega)_S$:

$$\mathbf{H}(\omega)_S = (\mathbf{H}(\omega)_A^{-1} \oplus \mathbf{H}(\omega)_B^{-1} \oplus \mathbf{H}(\omega)_C^{-1} \oplus \mathbf{H}(\omega)_D^{-1})^{-1}, \tag{17}$$

where $\oplus$ designates summing in terms of the finite-element summing of stiffness and mass matrices.

One should note that a priori modal and coordinate reduction is performed when only a portion of the FEM data for the A and B systems is used. However, additional co-ordinate reduction can be made directly on the FRF matrix, but not on the impedance matrix. The overall process for coupling the four systems is shown in Fig. 4.

3. Perturbation analysis and correlation

This section briefly presents the perturbation approach and least-squares updating of the model in a frequency domain, which serves as a tool to obtain the necessary modifications of the analytical model to correlate with the experimental model. Again, all the expressions refer to the

Table 1
Experimentally identified modal loss factors for subsystems A and B

	Modes (r) and corresponding η_r in %				
	1	2	3	4	5
Subsystem A	4.51	3.09	0.28	0.24	0.21
Subsystem B	0.14	0.14	0.098	—	—

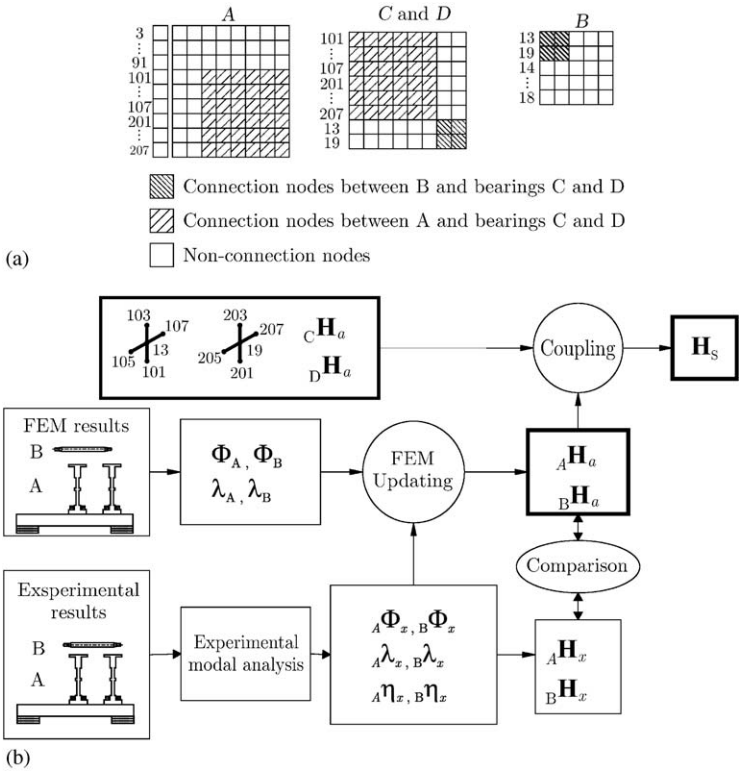

Fig. 4. Partitioning scheme for the four systems to be coupled using the standard FRF coupling method (a); algorithm of the coupling procedure (b). Index x denotes the experimental and index a the analytical model, respectively.

accelerance response model and in addition to a priori reduction from Section 2.2, the analytically coupled system model will be further spatially reduced (R) to achieve consistency with the experimental model – experimentally measured FRFs.

3.1. Least-squares model updating using FRF sensitivities

The well-known perturbation-based approach using the correlation principle and model updating (e.g. Ref. [26]) is used here to obtain the numerical algorithm for bearing-identification purposes. Applying a single-input *unit* force at coordinate j, $\mathbf{f}_j = \{0, 0, \ldots, 1, 0, \ldots, 0\}^{\mathrm{T}}$, to the analytical (FEM) and corresponding experimental models gives

$$\mathbf{Z}_u(\omega)\mathbf{H}_x(\omega)\mathbf{f}_j = \mathbf{I}_j = \mathbf{Z}_a(\omega)\mathbf{H}_a(\omega)\mathbf{f}_j, \tag{18}$$

where Z_u designates the updated impedance matrix (virtual mass) of the analytical system. Inserting

$$\mathbf{Z}_u(\omega) = \mathbf{Z}_a(\omega) + \Delta\mathbf{Z}_a(\omega), \quad \Delta\mathbf{Z}_a(\omega) \approx \sum_{i=1}^{N_p} \frac{\partial \mathbf{Z}_a(\omega)}{\partial p_i} \Delta p_i, \tag{19}$$

into Eq. (18) and rearranging gives

$$\mathbf{H}_a(\omega)\Delta\mathbf{Z}(\omega)\mathbf{H}_{x_j}(\omega) = \mathbf{H}_{a_j}(\omega) - \mathbf{H}_{x_j}(\omega) = \Delta\mathbf{H}_j(\omega). \tag{20}$$

Pre-multiplying Eq. (20) by $\mathbf{H}_a(\omega)$ yields the linear system of equations for calculating the $\Delta\mathbf{p}$ parameters

$$\mathbf{S}(\omega)\Delta\mathbf{p} = \Delta\mathbf{H}_{a_j}(\omega), \tag{21}$$

with

$$\mathbf{S}(\omega) = \mathbf{H}_a(\omega)\left[\frac{\partial\mathbf{Z}_a(\omega)}{\partial p_1}\mathbf{H}_{x_j}(\omega)\vdots\cdots\vdots\frac{\partial\mathbf{Z}_a(\omega)}{\partial p_{N_p}}\mathbf{H}_{x_j}(\omega)\right], \tag{22}$$

where a denotes the analytical model, u denotes the updated model, x denotes the experimental model, N_p denotes the number of parameters which $\mathbf{Z}_a(\omega)$, and therefore $\mathbf{H}_a(\omega)$, depend on, and $\mathbf{S}(\omega)$ denotes the *sensitivity matrix*.

If formulae (18)–(22) are to be used, the analytical system matrices have to be further reduced (R) to become consistent with the experimental matrix, $\mathbf{H}_x(\omega)$, and experimental vector, $\mathbf{H}_{x_j}(\omega)$. The reduction of the FRF matrices and their derivatives, such as $\mathbf{H}_a^R(\omega)$, can be applied directly by retaining only the remaining rows and columns. On the other hand, reduced impedance matrices and their derivatives (i.e., $\mathbf{Z}_a^R(\omega)$) can only be obtained indirectly using

$$\frac{\partial\mathbf{H}^R}{\partial p_i} = -\mathbf{H}^R\frac{\partial\mathbf{Z}^R}{\partial p_i}\mathbf{H}^R \quad \Rightarrow \quad \frac{\partial\mathbf{Z}^R}{\partial p_i} = -\mathbf{Z}^R\frac{\partial\mathbf{H}^R}{\partial p_i}\mathbf{Z}^R, \tag{23}$$

and

$$\mathbf{Z}^R = (\mathbf{H}^R)^{-1}. \tag{24}$$

In accordance with this approach, $\partial\mathbf{H}^R/\partial p_i$ is bearing-dependent only, and therefore is a sparse matrix; and as a consequence, $\partial\mathbf{Z}^R(\omega)/\partial p_i$ is a sparse matrix too.

In cases when the number of parameters, N_p, is larger than the number of rows in the reduced sensitivity matrix $\mathbf{S}(\omega)$, and if even the weighting is introduced, an over-determined system of equations in Eq. (22) is obtained. For that, additional frequency points can be invoked to expand system (22) (in reduced form—R):

$$\begin{bmatrix}\mathbf{S}^R(\omega_1)\\ \vdots \\ \mathbf{S}^R(\omega_{N_f})\end{bmatrix}\Delta\mathbf{p} = \begin{bmatrix}\Delta\mathbf{H}_j^R(\omega_1)\\ \vdots \\ \Delta\mathbf{H}_j^R(\omega_{N_f})\end{bmatrix}, \tag{25}$$

or in a more compact form (marked with $*$):

$$\mathbf{S}^{*R}(\omega)\Delta\mathbf{p} = \mathbf{H}_j^{*R}(\omega). \tag{26}$$

Since $\Delta\mathbf{p}$ are real-valued parameters, system (26) is further split into real (r) and complex (c) parts as

$$\mathbf{S}_r^{*R}(\omega)\Delta\mathbf{p} = \Delta\mathbf{H}_{jr}^{*R}(\omega), \tag{27}$$

$$\mathbf{S}_c^{*R}(\omega)\Delta\mathbf{p} = \Delta\mathbf{H}_{jr}^{*R}(\omega), \tag{28}$$

and only Eq. (27) is used to calculate $\Delta\mathbf{p}$. $\mathbf{S}^{*R}(\omega)$ is the expanded sensitivity matrix over the reduced analytical system, $\Delta\mathbf{p}$ are the parameter changes to be found, and $\Delta\mathbf{H}_{jr}^{*R}(\omega)$ is a vector of discrepancies between the analytical and corresponding experimental FRFs at selected frequency points.

Additional weighting can also be applied according to N_f frequency points, experimental FRF locations, or both, using the diagonal matrix $\mathbf{W}$:

$$\mathbf{W}^r\mathbf{S}^{*R}(\omega)\Delta\mathbf{p} = \mathbf{W}\Delta\mathbf{H}_{jr}^{*R}. \tag{29}$$

Finally, using the pseudo-inverse, the requested parameters are expressed in terms of the weighted least-squares approach as

$$\Delta\mathbf{p} = ((\mathbf{S}_r^{*R}(\omega))^{\mathrm{T}}\mathbf{W}\mathbf{S}_r^{*R}(\omega))^{-1}(\mathbf{S}_r^{*R}(\omega))^{\mathrm{T}}\mathbf{W}\Delta\mathbf{H}_{jr}^{*R}. \tag{30}$$

3.2. Parameter-identification algorithm

The bearing's stiffness matrix from Section 2.1 provides 15 different stiffness coefficients, regardless of the number of nodes used for the formulation of the FE model of the bearing (the 5-node FE model proposed). Additionally, 15 different damping parameters were applied with the initial values as

$$\mathbf{C}_{b5} = \beta_b\mathbf{K}_{b5}, \tag{31}$$

which together represent 30 bearing parameters to find, using Eq. (30). As the linearized equation (20) is only valid for small discrepancies between the analytical and experimental models in terms of $\Delta\mathbf{H}_{jr}^{*R}(\omega)$, the same restriction is applied to all the subsequent equations in Section 3.1. In this case the discrepancies, $\Delta\mathbf{H}_{jr}^{*R}(\omega)$, are up to 100% at the selected frequency locations with respect to the initial value of the numerical FRF. A special form of the iterative algorithm was introduced (Fig. 5) to estimate the required change of the updating parameters, $\Delta\mathbf{p}$.

The iteration algorithm used is shown in Fig. 5, where the additional relaxation parameter γ is introduced in order to improve convergence for cases of large discrepancies in $\Delta\mathbf{H}_{jr}^{*R}(\omega)$. In each iteration loop n, γ is calculated for every parameter p_k as

$$\gamma_{n_k} = \frac{a^b}{(|\Delta p_{n_k}/p_{n_k}| + a)^b}, \quad k = 1, \ldots, N_p, \tag{32}$$

where a and b represent the controlling parameters.

Together with the analytical models for A, B, C, and D, a corresponding experimental model is needed (the experimental object, which is called the experimental device) on which the modal identification can be performed. This is explained in the following section.

4. Experiment and results

4.1. Experimental device and FRF measurements

The special-purpose experimental device was made in accordance with the model shown in Fig. 3. The device allows two ball bearings, connected by a shaft, to be inserted and an axial

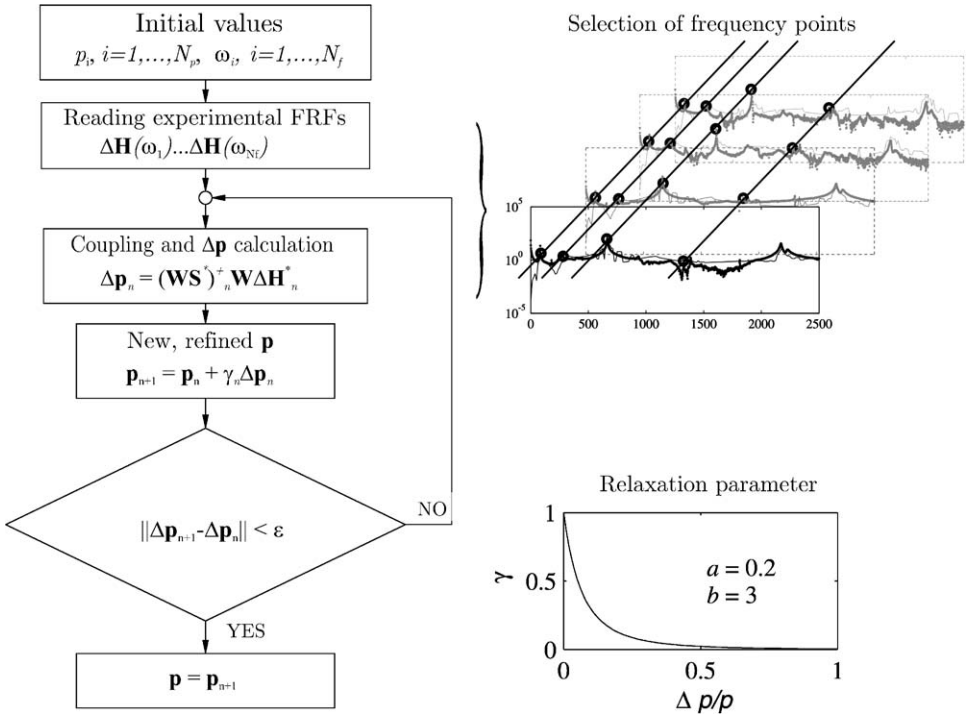

Fig. 5. The bearing-identification algorithm, based on the frequency domain least-squares updating correlation approach. The relaxation parameter is introduced to achieve better convergence by choosing appropriate parameters a and b.

pre-load to be applied to the bearings (Fig. 6). An impact test, using a hammer and an accelerometer, was used to measure the accelerance FRFs. The accelerometer was fixed at point 91, and the acceleration was measured in the z direction. The weight of the shaft, together with the partial weights of the two bearings, represented the constant radial pre-load on the two bearings. The influence of the shaft with two bearings on the FRF response of the device is shown in Fig. 7.

To observe the damping in subsystems A and B, separate FRF measurements were made on each subsystem, and the modal identification analysis was applied to extract the modal frequencies, the modal matrix, and the modal damping on the basis of the hysteretic and lightly damped dissipation model. Moreover, measurements of accelerance FRFs for the whole connected system were made at some points on the experimental device, from Fig. 6, and it was mainly those in the z direction that were used in subsequent analyses. For bearing-identification purposes, using the approach from Section 3, one row or column from the FRF matrix should be measured. Actually, all that needs to be measured is a driving-point measurement: $H_{91z-91z}$, in this case. To obtain better identification results, the measurement of additional FRFs, in addition to the driving-point, is needed (see Fig. 8). In other words, the system's reduction level (R) is dictated by the number of FRF measurements used.

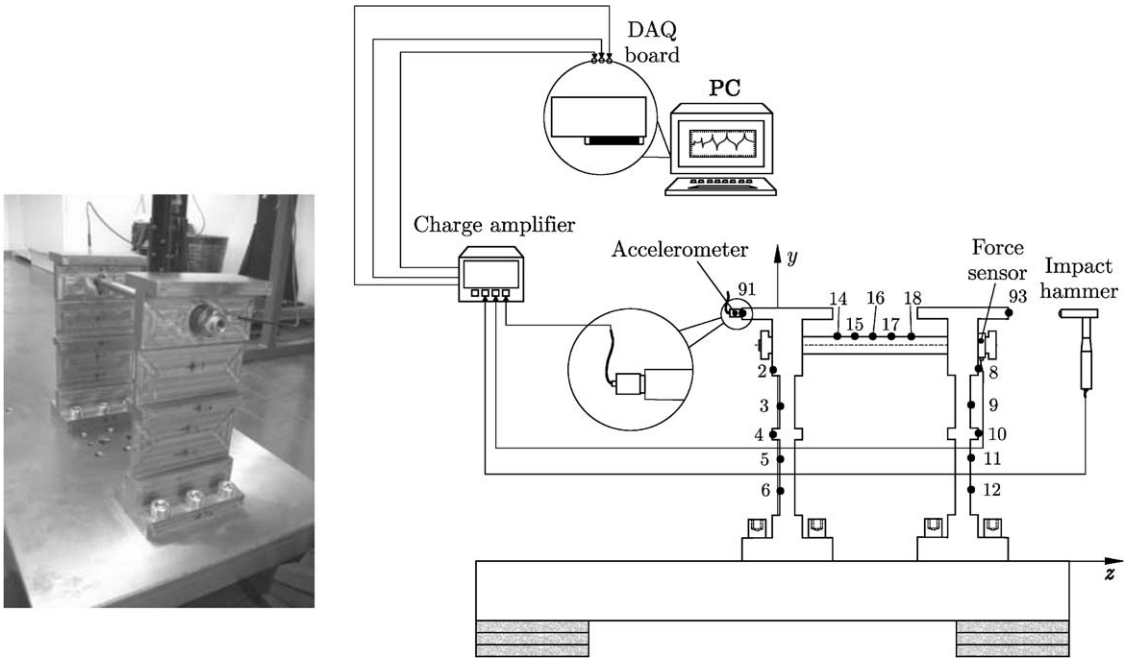

Fig. 6. Experimental setup for the FRF measurement.

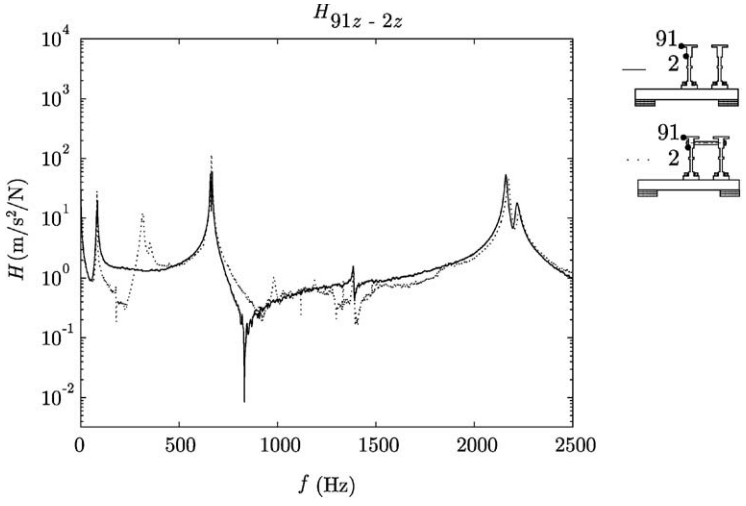

Fig. 7. The change of the H_{91z-2z} FRF, comparing measurement of FRF on subsystem A only (solid line) and FRF measurement on the connected system (dotted line).

4.2. Coupling results

With numerical accelerance FRFs data for A and B, which is obtained from a linear FEM analysis with applied identified damping (Table 1), and bearings' FRF according to the bearing

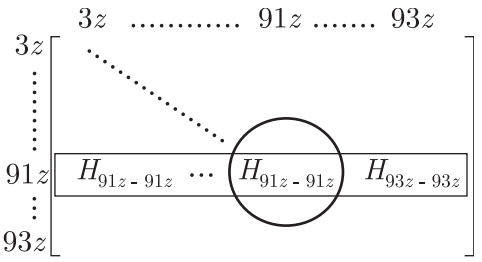

Fig. 8. Minimum required FRF measurement (circled), and suggested FRF measurement (boxed) for bearing-identification purposes.

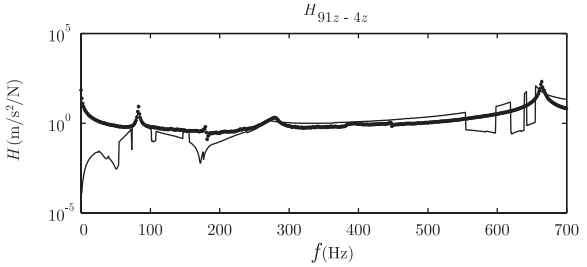

Fig. 9. Analytical (numerical) FRF of the connected system corresponding to the analytical pre-load force, $f_{zm} = 3$ N (solid line), and the experimental FRF with $f_{zm} = 18$ N (dotted line).

pre-load force, the coupling analysis can be used as described in Section 2.2 to obtain the connected system's FRF for any co-ordinate pair of provided subsystems and for any assumed bearing pre-load force. These numerical results can be directly compared to the experimental results (see, e.g., in Fig. 9).

From Fig. 9 it can be seen that the experimental overall FRF with the 18 N axial bearing pre-load corresponds to the analytical FRF with a smaller, 3 N, axial pre-load. The reason is that the bearing's axial force changes a lot, relative to the initial pre-load (18 N), causing the bearing stiffness to change when the system is vibrating (force-dependent stiffness, as discussed in Section 2.1). The analytical and experimental FRFs, both with 18 N, do not correlate well, as the analytical FRF tends to represent connections that are too stiff, resulting in a shift of the resonance peaks (especially the peak at $\approx$280 Hz, see Fig. 9). The same applies for other pre-load forces, when comparing the analytical and experimental FRF results. In this case, it turned out that the resonances around 85, 660, 2200, and 2250 Hz are almost insensitive to the change in the bearing's stiffness, while the resonance around 280 Hz (in the case with the experimental force of 18 N) is not.

Abrupt changes in the analytical FRF occur at some frequency points as a consequence of the rank-deficient system when calculating the coupled FRF. This could be avoided by using more sophisticated FRF coupling methods [27], but in such cases an appropriate update or even a change to couple more than two systems and to achieve an ability to derive a coupled system's impedance derivative matrix should be made.

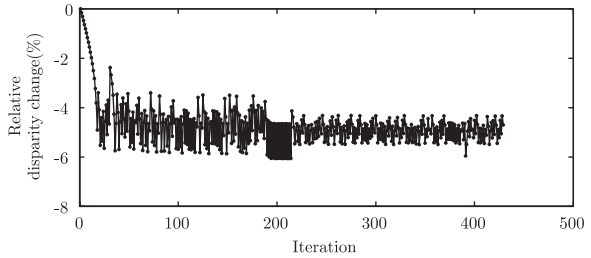

Fig. 10. The relative disparity change for the following frequency points: $\{80, 84, 260, 270, 275, 660, 665\}$. The experimental axial force for the two bearings was 18 N, and the corresponding analytical force (indirectly providing initial values for p_i, $i = 1, \ldots, 15$), was 3 N. The controlling parameters were chosen as: $a = 0.1$, $b = 4$.

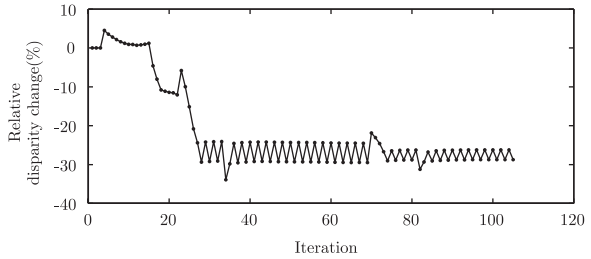

Fig. 11. The relative disparity change for the following frequency points: $\{80, 84, 260, 270, 275, 660, 665\}$. The experimental axial force for the two bearings was 5 N, and the corresponding analytical force (indirectly providing initial values for p_i, $i = 1, \ldots, 15$), was 0.3 N. The controlling parameters were chosen as: $a = 0.1$, $b = 4$.

4.3. Identification results

For identifying the bearing parameter, one row or column from the measured FRF matrix should be used and the corresponding, reduced analytical FRF information at $1, \ldots, N_f$ frequency points (Eqs. (26)–(30)). In this case, a row from the measurement FRF that corresponds to the $91z$ co-ordinate was used. Moreover, $3z, 4z, 9z, 10z, 91z$ FRF measurement co-ordinates were used. This implies that analytically coupled system has to be reduced correspondingly, in this case to dimension (5×5) in Eqs. (26)–(30).

Using the appropriate controlling parameters a and b to calculate the relaxation coefficient γ, as well as suitable frequency points, $\omega_1, \ldots, \omega_{N_f}$, and initial values for p_i, $i = 1, \ldots, 30$, convergence can be achieved by implementing the algorithm from Fig. 5. The disparity, which is a sum of the absolute differences between the experimental and corresponding analytical FRFs at selected frequencies points, and for the whole set of FRFs (see Fig. 5), can represent an estimation, as well as the quality, of the convergence in the identification process (see Figs. 10 and 11).

5. Conclusion

An integrated, generalized, indirect approach to the transmission of bearing vibrations was proposed, based on a m.d.o.f. system analysis of four subsystems. The frequency domain coupling

method was applied for the coupling of two analytically provided and updated subsystems with two bearings into a specially shaped system. Such a system provided the opportunity to compare experimental and analytical frequency response function results directly, which served as a tool to explore the appropriate bearing pre-load estimation, and, as a consequence, the validity of a bearing model. Moreover, such an approach is useful for large systems, where bearings represent only a connection between some parts of a large system, and serves as a convenient investigation of a bearing's influence on the overall dynamics of a system.

Additionally, using the perturbation approach in a correlation analysis, a bearing-identification algorithm was proposed, whose quality depends on the initial parameter values as well as on the bearing model. Selecting the appropriate initial values for the bearing parameters, the convergence in the identification algorithm can be obtained. The identification results show that to obtain a proper initial value for the bearing's stiffness and damping matrices using Eqs. (8) and (31), respectively, an appropriately smaller value can be used for the bearing pre-load estimation.

Acknowledgements

This research was supported by the Ministry of Science, Education and Sport of the Republic of Slovenia. The support of Domel, d.d. is also acknowledged.

Appendix. Nomenclature

a, b	controlling parameters for the calculation of the relaxation parameter
A_0	unloaded distance between the centers of inner and outer curvature
$A(\psi_j)$	loaded distance between the centers of inner and outer curvature
$\mathbf{C}_{b5}$	5-node bearing's viscous damping matrix
d	ball diameter
$\mathbf{D}$	hysteretic damping matrix
$\mathbf{F}$	generalized force vector
$\mathbf{f}_{bm}$	mean bearing force vector
$\mathbf{f}_j$	unit-force vector
f_{xm}, f_{ym}, f_{zm}	mean bearing forces in x, y, and z directions
$\mathbf{H}$, $\mathbf{H}_j$	accelerance FRF matrix and the jth column from the accelerance FRF matrix, respectively
H_{jk}	accelerance FRF which corresponds to input (k) and output (j) location
$\mathbf{K}_{b2}$	2-node bearing stiffness matrix
$\mathbf{K}_{b5}$	5-node bearing stiffness matrix
$\mathbf{K}_{bm}$	mean bearing stiffness matrix
K_n	load–deflection coefficient of the ball
k_{xx}	bearing stiffness coefficient
m_{xm}, m_{ym}	mean bearing moment about x- and y-axis
$\mathbf{M}_{b2}$	2-node bearing mass matrix
N_f	number of frequency points

N_p	number of parameters
$\mathbf{p}, \Delta\mathbf{p}$	vector of parameters; vector of parameters' changes
r_j	distance from the bearing center axis to inner curvature center
$\mathbf{q}_{bm}$	mean bearing displacement vector
Q	normal force load (N)
$\mathbf{S}$	sensitivity matrix
$\mathbf{W}$	diagonal weighting matrix
$\mathbf{Z}$	impedance matrix (virtual mass)
α, β	factors of proportional damping
β_b	factor of bearing's proportional, viscous damping
α_j	jth contact angle
δ	deflection; displacement
δ_{n_j}	displacement of the ball in the normal (z) direction
δ_{r_j}	displacement of the ball in the radial direction
η	modal damping loss factor
γ	relaxation parameter
ω	angular frequency (rad/s)
$\boldsymbol{\omega}_r^2$	diagonal matrix of squared natural frequencies ($\mathrm{rad}^2/\mathrm{s}^2$)
ϕ	a term from the mass-normalized modal matrix
$\boldsymbol{\Phi}$	mass-normalized modal matrix
ψ_j	jth ball's angle, measured from the positive x-axis

References

[1] E. Krämer, *Dynamics of Rotors and Foundations*, Springer, Berlin, 1993.
[2] T.A. Harris, *Rolling Bearing Analysis*, Wiley, New York, 1966.
[3] T.C. Lim, R. Singh, Vibration transmission through rolling element bearings, 1. bearing stiffness formulation, *Journal of Sound and Vibration* 139 (2) (1990) 179–199.
[4] T.C. Lim, R. Singh, Vibration transmission through rolling element bearings, 2. system studies, *Journal of Sound and Vibration* 139 (2) (1990) 201–225.
[5] T.C. Lim, R. Singh, Vibration transmission through rolling element bearings, 4. statistical energy analysis, *Journal of Sound and Vibration* 153 (1) (1992) 37–50.
[6] C.H. Chen, K.W. Wang, Y.C. Shin, An integrated approach toward the dynamic analysis of high-speed spindles. 1. system model, *Journal of Vibration and Acoustics—Transactions of the American Society of Mechanical Engineers* 116 (4) (1994) 506–513.
[7] C.H. Chen, K.W. Wang, An integrated approach toward the dynamic analysis of high-speed spindles. 2. dynamics under moving end load, *Journal of Vibration and Acoustics—Transactions of the American Society of Mechanical Engineers* 116 (4) (1994) 514–522.
[8] T.J. Royston, I. Basdogan, Vibration transmission through self-aligning (spherical) rolling element bearings: Theory and experiment, *Journal of Sound and Vibration* 215 (5) (1998) 997–1014.
[9] J.R. Bilodeau, *Dynamic event monitoring across tapered roller bearings*, Masters Thesis, Colorado State University, Fort Collins, CO, 1996.
[10] T.E. Rook, R. Singh, Structural intensity calculations for compliant plate-beam structures connected by bearings, *Journal of Sound and Vibration* 211 (3) (1998) 365–387.

[11] R.W. Stephenson, K.E. Rouch, Generating matrices of the foundation structure of a rotor system from test data, *Journal of Sound and Vibration* 154 (3) (1992) 467–484.
[12] Y.A. Khulief, M.A. Mohiuddin, On the dynamic analysis of rotors using modal reduction, *Finite Elements in Analysis and Design* 26 (1) (1997) 41–55.
[13] C.X. Mao, Q.H. Qin, Coupled torsional-flexural vibration of shaft systems in mechanical engineering. 2. fe-tm impedance coupling method, *Computers and Structures* 58 (4) (1996) 845–849.
[14] D.M. Shamine, S.W. Hong, Y.C. Shin, An in situ modal-based method for structural dynamic joint parameter identification, *Proceedings of the Institution of Mechanical Engineers Part C—Journal of Mechanical Engineering Science* 214 (5) (2000) 641–653.
[15] N. Lynagh, H. Rahnejat, M. Ebrahimi, R. Aini, Bearing induced vibration in precision high speed routing spindles, *International Journal of Machine Tools and Manufacture* 40 (4) (2000) 561–577.
[16] S.A. Spiewak, T. Nickel, Vibration based preload estimation in machine tool spindles, *International Journal of Machine Tools and Manufacture* 41 (4) (2001) 567–588.
[17] R. Tiwari, N.S. Vyas, Parameter estimation in imbalanced non-linear rotor-bearing systems from random response, *Journal of Sound and Vibration* 208 (1) (1997) 1–14.
[18] F.M.A. El Saeidy, Finite element modeling of a rotor shaft rolling bearings system with consideration of bearing nonlinearities, *Journal of Vibration and Control* 4 (5) (1998) 541–602.
[19] J. Kicinski, R. Drozdowski, P. Materny, Nonlinear model of vibrations in a rotor-bearings system, *Journal of Vibration and Control* 4 (5) (1998) 519–540.
[20] J.K. Dutt, B.C. Nakra, Dynamics of rotor shaft system on flexible supports with gyroscopic effects, *Mechanics Research Communications* 22 (6) (1995) 541–545.
[21] I. Basdogan, T.J. Royston, A theoretical and experimental study of the vibratory dynamics of high-precision optical positioning systems, *Journal of Vibration and Control* 5 (2) (1999) 195–216.
[22] M. Aleyaasin, M. Ebrahimi, R. Whalley, Vibration analysis of distributed-lumped rotor systems, *Computer Methods in Applied Mechanics and Engineering* 189 (2) (2000) 545–558.
[23] J.A. Wensing, On The Dynamics of Ball Bearings, Thesis/Dissertation, University of Twente, Enschede, The Netherlands, 1998.
[24] R.B. Bhat, Component mode synthesis in modal testing of structures, *Journal of Sound and Vibration* 101 (2) (1985) 271–272.
[25] H. Fang, B. Yang, Modelling, synthesis and dynamic analysis of complex flexible rotor systems, *Journal of Sound and Vibration* 211 (4) (1998) 571–592.
[26] N.M.M. Maia, J.M.M. Silva, *Theoretical and Experimental Model Analysis*, Research Studies Press, Taunton, 1997.
[27] Y. Ren, C.F. Beards, On substructure synthesis with frf data, *Journal of Sound and Vibration* 185 (5) (1995) 845–866.